## EDGE ARTICLE

# Switching between photochromism and photoluminescence in Schiff base derivatives by molecular design of end groups

Qilong Zhang, [ID] †*[ab] Xu Zhou, [ID] †[a] Xiaofeng Shan,†[a] Fa He,[b] Yuwei Bao,[a] Hong Xu,[a] Chun Zhu [ID] *[b] and Bixue Zhu [ID] *[b]

Ensuring the security and reliability of information has increasingly become a key issue for modern society, placing greater demands on encryption technologies and anti-counterfeiting materials. Therefore, the development of intelligent responsive materials with multi-mode encryption and protection capabilities has become crucial. In this study, an aldehyde–amine exchange approach was applied based on the traditional ESIPT–ISO (Excited state intramolecular proton transfer and *cis* to *trans* isomerization) color-switching mechanism of salicylaldehyde-aniline Schiff bases. The reaction between tetraphenylethyl salicylaldehyde and aniline derivatives generated eight Schiff base compounds. Five of these compounds displayed UV-triggered color change in the solid phase, whereas the other three exhibited fluorescence emission in solid form. Spectroscopic analysis, theoretical computation, and crystal-structure characterization clarified the mechanisms responsible for both color variation and stability. The stable compounds showed characteristic stacking configurations, and the hydroxyl groups formed weak interactions with nearby atoms, restricting the ESIPT transition and preventing color change under UV irradiation. This work presents the first systematic report on the effect of substituent variation on the ESIPT–ISO process, illustrating how weak interactions and packing modes can inhibit ESIPT. It also represents the first study describing substituent influences on the reverse ESIPT–ISO reaction. Finally, five UV-responsive color-switching materials were developed into color-shifting inks. Through pad and screen printing, these inks enabled encrypted information and anti-counterfeiting features on paper, inorganic, and fiber substrates, maintaining long-term stability for up to three years. Moreover, by utilizing differences in fading times among the photochromic molecules, color-changing inks were overprinted in specific sequences. Upon UV activation, this approach allowed multi-level time-space encryption and anti-counterfeiting of data.

## Introduction

In the big data era, the methods and channels through which people obtain information have become increasingly varied and convenient.[1–3] However, maintaining the authenticity and security of information has gradually become a major issue, creating higher requirements for encryption techniques and anti-counterfeiting materials.[4–6] Thus, studies on encrypted anti-counterfeiting materials have become particularly important, with intelligent responsive systems capable of multi-mode encryption and protection being of prime significance.[7,8]

At present, several photochromic, phosphorescent, and fluorescent materials are employed in the anti-counterfeiting field.[9–13] Among these, the development of photochromic compounds has attracted wide attention in optical encryption and security applications.[14–16] In recent years, various representative photochromic molecules—such as spiropyran, azobenzene, and aromatic radical derivatives—have been reported and widely applied for information protection and verification.[17–19] Nevertheless, most photochromic materials experience restricted molecular rotation and motion in the aggregated state, hindering the formation of optical isomers. As a result, their photochromic response generally appears only in the dissolved state.[20,21] Additionally, the extent of color change in aggregated photochromic systems is governed by crystallization, making synthesis procedures laborious and time-consuming.[22,23] The differing color-switching behaviors between crystalline and amorphous states further complicate the interpretation of mechanisms, limiting progress in understanding and applying photochromic systems for encryption

*[a]School of Basic Medical Sciencese, Key Laboratory of Macrocyclic and Supramolecular Chemistry of Guizhou Province, Guizhou Medical University, Guiyang 561113, PR China. E-mail: gzuqlzhang@126.com*

*[b]Guizhou Key Laboratory of Macrocyclic and Supramolecular Chemistry, School of Chemistry and Chemical Engineering, Guizhou University, Guiyang 550025, PR China. E-mail: czhu2014@163.com; bxzhu@gzu.edu.cn*

† The authors contributed equally to this study.

and anti-counterfeiting.[24] Organic crystals, with well-defined structures and molecular arrangements, provide ideal models for analyzing how intermolecular forces and packing affect solid-state luminescence.[25–27] Therefore, designing photochromic materials that perform efficiently in both amorphous and crystalline forms—with easy preparation, quick response, and strong stability—represents highly valuable research. Such materials can also provide clear experimental evidence for understanding the origin of color transformation.

Salicylaldehyde-aniline Schiff bases constitute a class of organic molecules known for their solid-state photochromic behavior. Due to their simple synthesis and ease of structural modification, they are widely used to construct photoresponsive systems for encryption-decryption and anti-counterfeiting applications.[28–31] The photochromic mechanism in these compounds generally involves a two-step process: "enol → iso → anti" (ESIPT + ISO). In this mechanism, excited-state intramolecular proton transfer (ESIPT) allows the enol form to convert into the iso tautomer, producing a red-shifted absorption band, followed by conversion of the ISO form to the anti-isomer, leading to further absorption enhancement.[32,33]

During crystallization, salicylaldehyde-aniline Schiff bases tend to form six-membered intramolecular hydrogen-bonded rings, promoting the ESIPT transition. Consequently, earlier studies concentrated on tuning the ISO process to explore photochromism, assuming ISO as the main factor governing the phenomenon.[34,35] To strengthen the ISO transition, tetraphenylvinyl units with strong steric effects were introduced into the Schiff base framework. This modification disrupted π–π stacking, induced active molecular motion, and triggered photochromism.[29] However, later research revealed that ISO alone does not solely determine photochromic behavior. The ESIPT process also plays a vital role in influencing the ESIPT–ISO mechanism. For example, Tang and Cai (2021) incorporated alicyclic substituents into salicylaldehyde-aniline Schiff bases and proposed that ESIPT–ISO cooperative effects enhance photochromism.[36,37] In a subsequent study (2023), they introduced triphenylamine groups with propeller-like configurations, demonstrating that crystallization and rapid precipitation methods affect hydrogen bond formation and thus control the ESIPT process. Their work identified ESIPT as the primary factor controlling the ESIPT–ISO coupling mechanism.[38] Meanwhile, various studies have shown that aggregation states can significantly influence the ESIPT process. With advances in aggregate science, it has been recognized that some aggregated forms exhibit properties superior to their monomeric counterparts, while others display synergistic enhancement where 1 + 1>2. Aggregation-Induced Emission (AIE) systems are the most representative examples of this behavior.[39–43] Although the importance of aggregate-level understanding is now well acknowledged, practical methods for analyzing complex internal interactions and establishing clear structure–property correlations—particularly regarding new properties emerging upon aggregation—remain insufficient. Therefore, expanding theoretical frameworks and research methods in aggregate science to enable deeper investigation in this area remains an essential goal.

Triphenylamine and tetraphenylethylene, owing to their twisted molecular structures, are widely employed in the design and construction of AIE molecules.[44–52] Introducing triphenylamine and tetraphenylethylene into salicylaldehyde-aniline Schiff base compounds to construct AIE-type systems yields more pronounced photochromic properties. Chi, Ni, and Hou reported three examples of ESIPT-type salicylaldehyde-aniline Schiff base AIE compounds based on a tetraphenylethylene skeleton. All exhibited significant color changes under UV irradiation and spontaneously reverted to their original state upon cessation of light exposure. These advantages offer considerable potential for practical applications.[53–55]

Previous studies on the construction of triphenylamine- and tetraphenylethylene-based salicylaldehyde-aniline Schiff base photochromic compounds primarily involved reactions between the amino group on the triphenylamine or tetraphenylethylene skeleton and various types of salicylaldehyde.[34–37,53–55] Given the relatively limited range of salicylaldehyde derivatives with different substituents, few studies have examined the influence of substituents on the ESIPT–ISO process. What would be the photochromic behavior of tetraphenylethylene salicylaldehyde-aniline Schiff base compounds if tetraphenylethylene salicylaldehyde were reacted with different anilines through an aldehyde–amine exchange strategy? If this strategy successfully constructs photochromic tetraphenylethyl salicylaldehyde-aniline Schiff base compounds, it would expand the possibilities for photochromic molecular design. Aromatic anilines with diverse substituents are relatively inexpensive and easy to synthesize, enabling more convenient investigation of substituent effects on the ESIPT–ISO process.

Although the photochromic mechanism of salicylaldehyde-aniline Schiff base photochromic compounds is well established, the fundamental cause of the process remains unclear.[28–37,53–55] To date, no studies have examined how substituents influence either the ESIPT–ISO or the reverse ESIPT–ISO process. Furthermore, few investigations have explored the impact of single-molecule versus aggregated states on the ESIPT–ISO mechanism. The factors governing how aggregation affects photochromic properties also remain uncertain, necessitating further research to develop strategies for controlling photochromic behavior.

Based on this rationale, we employed an aldehyde–amine exchange strategy to synthesize eight tetraphenylethyl salicylaldehyde-aniline Schiff base derivatives by reacting 2-hydroxy-5-(1,2,2-triphenylvinyl)benzaldehyde with eight anilines bearing different substituents. The luminescent properties of these compounds were systematically investigated. All the compounds exhibited AIE effects. Theoretical calculations indicated that in the single-molecule state, all eight molecules are capable of undergoing the ESIPT–ISO process, making them photoresponsive. However, in the solid aggregate state, only **TPE-P**, **TPE-*p*-tBuP**, **TPE-*o*-FP**, **TPE-*p*-FP**, and **TPE-*p*-MP** exhibited significant color changes (from pale yellow to red) upon UV irradiation in both crystalline and amorphous states through the ESIPT–ISO process. Substituents modulate the reverse ESIPT–ISO process, and after UV-induced red coloration, the

fading times decrease in the order: **TPE-*p*-tBuP**, **TPE-*o*-FP**, **TPE-*p*-FP**, **TPE-P**, and **TPE-*p*-MP**. The longest fading time was 16 min for **TPE-*p*-tBuP**, while **TPE-*p*-MP** and **TPE-P** exhibited the shortest fading time of 5 s. **TPE-*p*-MOP**, **TPE-*o*-BrP**, and **TPE-*p*-NO₂P** maintain their color under illumination and exhibit fluorescence in the solid state.

Crystal structures revealed that **TPE-P**, **TPE-*p*-tBuP**, **TPE-*o*-FP**, **TPE-*p*-FP** and **TPE-*p*-MP** adopt a single conformation, termed the "X" conformation. The molecular packing patterns of **TPE-P**, **TPE-*o*-FP**, **TPE-*p*-FP** and **TPE-*p*-MP** are essentially identical. In these structures, hydroxyl groups form only O1–H1···N1 hydrogen bonds and are unaffected by other weak interactions, favoring the ESIPT process. The three photostable compounds, **TPE-*p*-MOP**, **TPE-*o*-BrP** and **TPE-*p*-NO₂P**, adopt a distinct structural arrangement referred to as the "Y" conformation. Within these molecules, the hydroxyl groups establish intra-molecular O1–H1···N1 hydrogen bonds with the nitrogen atom of the C=N bond and simultaneously participate in weak secondary interactions with nearby atoms, thereby suppressing the ESIPT process. As a result, these compounds exhibit no observable color change under UV irradiation. This study provides the first evidence of substituent-dependent regulation of the ESIPT–ISO mechanism, highlighting the constraining role of weak intermolecular interactions and molecular stacking patterns on ESIPT behavior. It also represents the first study examining substituent effects on the reverse ESIPT–ISO process.

Finally, five color-changing materials were formulated into color-shifting inks. Through pad printing and screen printing, information encryption and anti-counterfeiting were achieved on paper, inorganic, and fiber substrates. These applications remained effective even after three years of storage. Furthermore, exploiting the differing fade times of photochromic compounds, these materials were cross-printed in specific sequences to create time-dependent color transitions. Upon UV illumination, this technique enables multimodal spatiotemporal encryption and anti-counterfeiting of data.

## Results and discussion

### Design and synthesis of compounds

Inspired by the photoresponsive behavior of Schiff base derivatives obtained from reactions between amino groups on tri-phenylamine or tetraphenylethylene frameworks and various salicylaldehydes, eight new tetraphenylethylene salicylaldehyde-aniline Schiff base compounds were synthesized through an aldehyde–amine exchange method. In this approach, 2-hydroxy-5-(1,2,2-triphenylvinyl)benzaldehyde was reacted with eight anilines bearing different substituents to produce the corresponding Schiff bases (Scheme 1). Details of the synthesis routes and characterization data are provided in the SI (Fig. S1–S24). Among these, **TPE-P**, **TPE-*p*-tBuP**, **TPE-*o*-FP**, **TPE-*p*-FP** and **TPE-*p*-MP** exhibit photochromic properties, while **TPE-*p*-MOP**, **TPE-*o*-BrP** and **TPE-*p*-NO₂P** demonstrate photo-luminescent properties.

### Physical properties of light

The UV-vis absorption spectra of all compounds in DMSO solution were recorded (Fig. 1a). The spectra of the eight derivatives displayed high similarity, attributed to their comparable molecular frameworks, although the molar extinction coefficients varied slightly due to substituent effects (Table S1). Since each compound contained the classical AIE fluorophore tetraphenylethylene, it was anticipated that they would exhibit AIE characteristics. Accordingly, fluorescence spectra
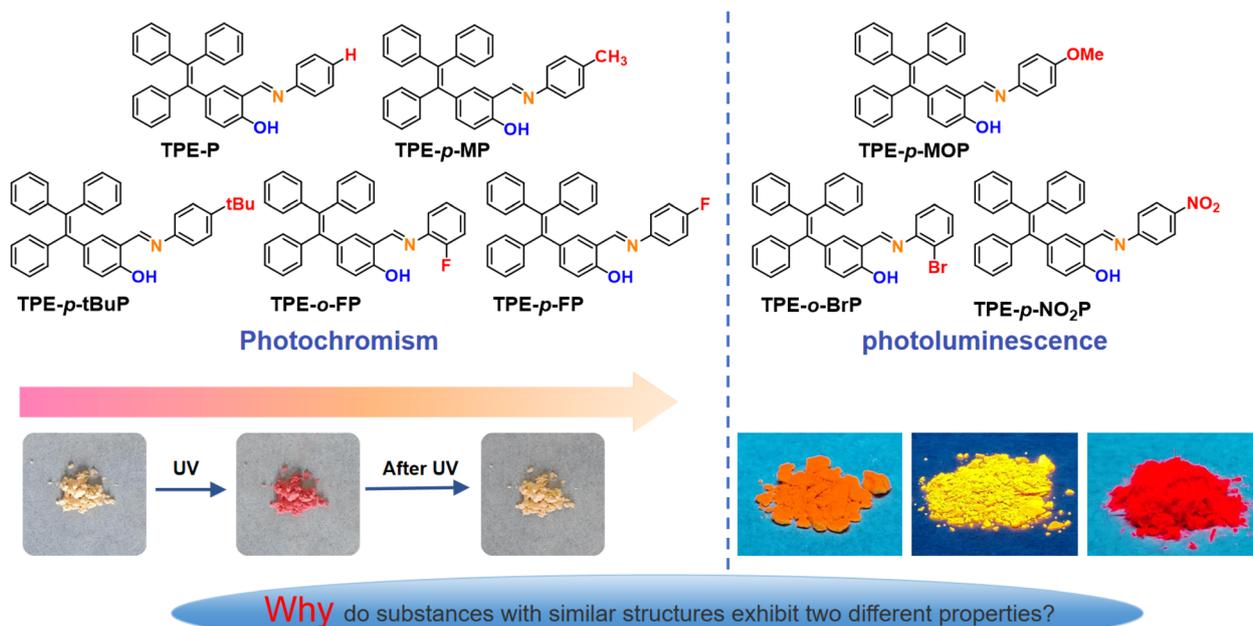


**Scheme 1** Eight synthetic tetraphenylethylsalicylaldehyde-aniline Schiff base compounds and their two distinct properties.
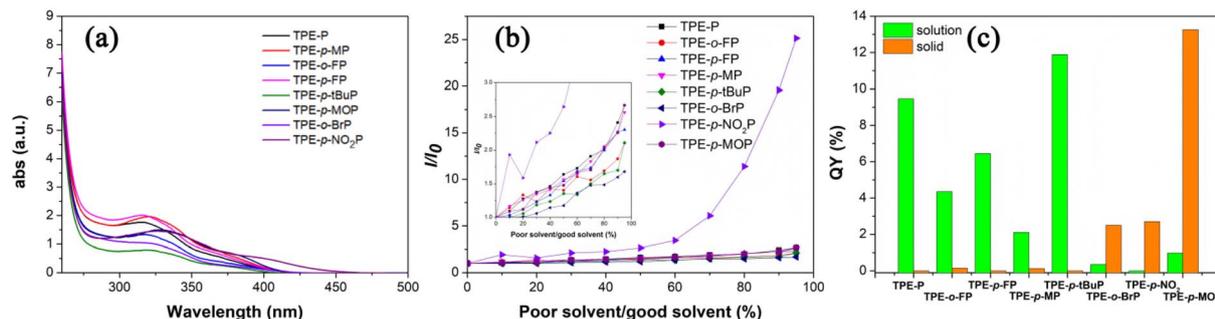
**Fig. 1** (a) UV-vis absorption spectrum of the compound in DMSO solution (10 μM); (b) fluorescence behavior of the compound in mixed DMSO/water solvents at different ratios; (c) fluorescence quantum yield of the compound in DMSO solution and in the solid state.

were measured in mixed solvents with varying ratios of DMSO and water (Fig. 1b and S25). As expected, all compounds exhibited clear AIE behavior.

To further verify this property, fluorescence quantum yields were determined both in DMSO and in the solid state. An interesting contrast was observed: the solid-state quantum yields of **TPE-*p*-MOP**, **TPE-*o*-BrP** and **TPE-*p*-NO₂P** were higher than their solution values, consistent with the typical AIE phenomenon. In contrast, **TPE-P**, **TPE-*p*-tBuP**, **TPE-*o*-FP**, **TPE-*p*-FP** and **TPE-*p*-MP** showed lower solid-state quantum yields than in solution (Fig. 1c). This result is clearly related to the fact that the solid compound exhibits two distinct properties under ultraviolet light irradiation: photochromism and photoluminescence. Further studies revealed that when in solid powder form, **TPE-P**, **TPE-*p*-tBuP**, **TPE-*o*-FP**, **TPE-*p*-FP** and **TPE-*p*-MP** undergo a color change from white or pale yellow to red upon exposure to UV light. When UV exposure ceased, the colors gradually reverted to their original shades, with fading times varying significantly. The longest fading time was recorded for **TPE-*p*-tBuP** (16 min), while **TPE-*p*-MP** returned to its initial color within 5 s. The order of fading time was **TPE-*p*-tBuP** > **TPE-*o*-FP** > **TPE-*p*-FP** > **TPE-P** ≈ **TPE-*p*-MP** (Fig. S26). Solid-state UV spectroscopy further confirmed these results (Fig. S27). According to literature reports, salicylaldehyde-aniline Schiff base compounds readily undergo photochromic changes under UV irradiation, exhibiting an ESIPT + ISO process.[31–34,50–52] Therefore, we speculate that the low solid-state quantum yields of **TPE-P**, **TPE-*p*-tBuP**, **TPE-*o*-FP**, **TPE-*p*-FP** and **TPE-*p*-MP** result from the energy absorbed by the molecules being utilized for photochromism.

## Crystal structures of compounds

The above research findings indicate that the powders of compounds **TPE-P**, **TPE-*p*-tBuP**, **TPE-*o*-FP**, **TPE-*p*-FP** and **TPE-*p*-MP** exhibit photochromic properties. Do their crystals also possess photochromic properties? Organic crystals possess well-defined structures and molecular arrangements, providing an ideal model system for investigating the influence of intermolecular forces and molecular ordering on solid-state luminescent properties. If the crystalline forms of these compounds also exhibit photchromic behavior, analyzing their crystal structures would significantly facilitate elucidating the

photochromic mechanism and identifying factors influencing color change. Single crystals of all eight derivatives were successfully obtained through slow solvent evaporation and analyzed by single-crystal X-ray diffraction. The X-ray crystallographic parameters of the 8 compounds are presented in Tables S2 and S3. Among these, five compounds—**TPE-P**, **TPE-*p*-tBuP**, **TPE-*o*-FP**, **TPE-*p*-FP** and **TPE-*p*-MP**—showed photochromism (Fig. 5b), whereas **TPE-*p*-MOP**, **TPE-*o*-BrP** and **TPE-*p*-NO₂P** remained non-photochromic. These results demonstrate that both crystalline and amorphous phases can undergo color change, providing direct structural evidence for analyzing the photochromic mechanism.

The crystal structure reveals that compounds **TPE-P**, **TPE-*p*-tBuP**, **TPE-*o*-FP**, **TPE-*p*-FP** and **TPE-*p*-MP** exhibit the "X" conformation (Fig. 2a), while **TPE-*p*-MOP**, **TPE-*o*-BrP** and **TPE-*p*-NO₂P** adopt the "Y" conformation (Fig. 2b). Because tetraphenylethylene can vibrate freely in solution, both configurations are possible. Interestingly, photochromic solids consistently adopt the "X" conformation (Fig. S28), whereas non-photochromic solids take the alternative "Y" form (Fig. S29), confirming that conformation and packing arrangement are decisive factors for photochromic behavior.

Next, we conducted a detailed analysis of the packing arrangement and interactions within the compound crystals. The crystal structure reveals that the hydroxyl groups on the five photochromic molecules form only O1–H1⋯N1 hydrogen bonds, with no other weak interactions affecting the hydroxyl
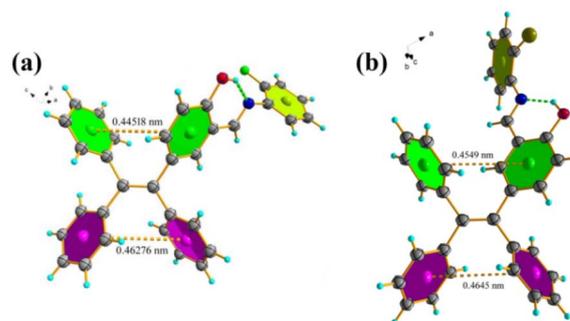


**Fig. 2** Two distinct molecular conformations: (a) "X" conformation (taking **TPE-*o*-FP** as an example); (b) "Y" conformation (taking **TPE-*o*-BrP** as an example).

groups. This configuration enables proton transfer in the photoexcited state. Additionally, owing to their essentially identical conformations, **TPE-P**, **TPE-*o*-FP**, **TPE-*p*-FP**, and **TPE-*p*-MP** exhibit C12–H12⋯Cg1, C13–H13⋯Cg3, C18–H18⋯Cg5, C27–H27⋯ Cg2, C30–H30⋯Cg1, and C32–H32⋯Cg2 interactions at six identical positions with other molecules, exhibiting essentially identical molecular packing patterns. Substituents exert no influence on their packing arrangements (Fig. 3a and S31).

Unlike the previous four photochromic molecules, **TPE-*p*-tBuP** exhibits only two C17–H17⋯Cg1 and C36–H36⋯Cg1 interactions (Fig. 3b). Indicating that the stacking arrangement of **TPE-*p*-tBuP** differs from that of the previous four molecules. In **TPE-*p*-tBuP**, the phenyl rings containing *tert*-butyl groups exhibit C30–H30⋯C33 and C33–H33⋯C30 intermolecular atypical hydrogen bonding interactions (Fig. 3c). Furthermore, the benzene rings are disordered, and the *tert*-butyl group is relatively large. Consequently, after forming the anti-ketone form upon light exposure, the return to the *cis*-ketone form and subsequent reverting to the enol form occurs relatively slowly. This is likely the reason why **TPE-*p*-tBuP** turns red upon light exposure and takes the longest to revert to its initial color after light exposure ceases. The weak interactions of photochromism compounds are shown in Table S4

The hydroxyl group of compound **TPE-*p*-NO₂P** forms not only an O1–H1⋯N1 hydrogen bond but also a C29–H29⋯O1 intermolecular hydrogen bond with an adjacent molecule, creating a dimer (Fig. 3d). This dimer forms a 1D structure *via* an atypical C32–H32⋯O3 hydrogen bond. The 1D structure expands into a 2D channel structure *via* C19–H19⋯O2 weak interactions

(Fig. S32c). Additionally, **TPE-*p*-NO₂P** forms interactions with two surrounding molecules: C5–H5⋯Cg3 and C4–H4⋯Cg2 (Fig. S33a). The hydroxyl group of **TPE-*o*-BrP**, in addition to forming the O1–H1⋯N1 hydrogen bond, interacts with another adjacent molecule *via* a C16–H16⋯O1 intermolecular hydrogen bond, thereby expanding into a 1D structure (Fig. S32a). Additionally, the **TPE-*o*-BrP** forms C3–H3⋯Cg2, C11–H11⋯Cg5, C19–H19⋯Cg4, and C25–H25⋯Cg2 interactions with four surrounding molecules (Fig. S33b). The hydroxyl group of **TPE-*p*-MOP**, besides forming an O1–H1⋯N1 hydrogen bond, also exhibits a weak C18–H18⋯O1 intermolecular hydrogen bond interaction with another adjacent molecule (Fig. S32b). Additionally, **TPE-*p*-MOP** forms interactions with three surrounding molecules: C3–H3⋯Cg2, C11–H11⋯Cg1, C17–H17⋯Cg4, C33–H33⋯Cg5, and C34–H34⋯Cg4 (Fig. S33c). In summary, besides the O1–H1⋯N1 hydrogen bond between the hydroxyl group and the nitrogen atom of the C=N double bond, the hydroxyl group in the three photoluminescent molecules also forms weak interactions with other atoms (Table S5). This restricts proton transfer at the hydroxyl group and limits the ESIPT process, so illumination does not cause color change but instead induces luminescence. Furthermore, analysis of the distances between the hydroxyl group and the nearest atoms in adjacent molecules reveals that the hydroxyl group in photochromic molecules is farther from its nearest neighbors than in photoluminescent molecules (Fig. S30 and Table S6). This indicates relatively looser packing, providing a more permissive environment for ESIPT. Consequently, these molecules exhibit photochromism.
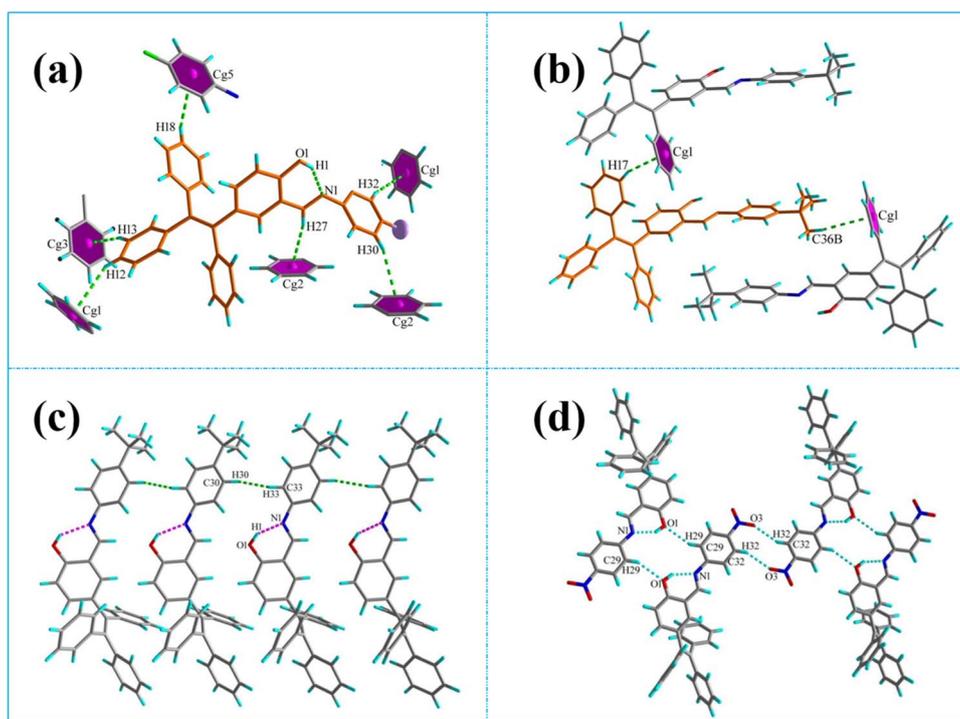


Fig. 3 (a) Schematic illustration of C–H⋯Cg interactions present in TPE-P, TPE-*o*-FP, TPE-*p*-FP, and TPE-*p*-MP; (b) C–H⋯Cg intermolecular interactions and (c) C–H⋯C atypical intermolecular hydrogen bonds in TPE-*p*-tBuP; (d) O–H⋯N hydrogen bonds between molecules of TPE-*p*-NO₂P.

Since the photochromic and photoluminescent properties of both crystalline and amorphous states are consistent, we conclude that the color-changing and luminescent mechanisms in the amorphous state are identical to those in the crystalline state. We further examined the morphology of powder samples *via* SEM (Fig. S34–S35). SEM observations revealed that the solid powder microstructures of all eight compounds exhibited various regular morphologies, indicating that the powder directly precipitated from the reaction formed micro- and nanocrystalline structures. Therefore, the color-changing mechanism and luminescence mechanism are consistent for both crystalline and amorphous states.
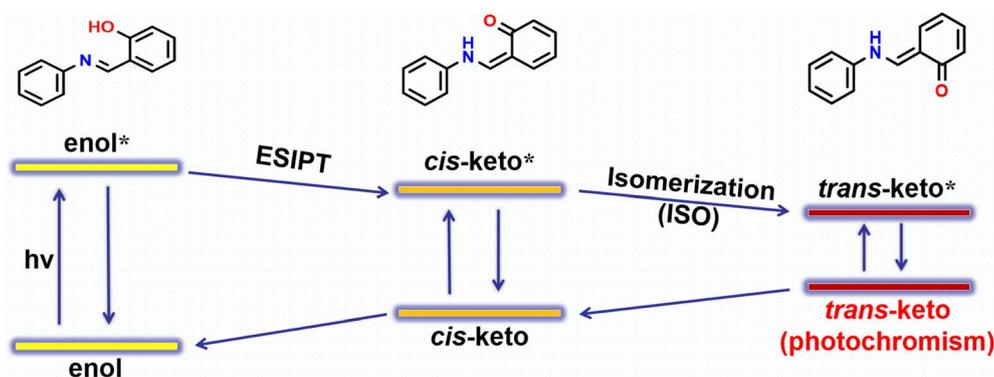
## Investigation of the photochromic mechanism

The crystal structure reveals that the hydroxyl group on the non-color-changing compound molecule forms weak interactions with other atoms, thereby restricting the ESIPT process. This leads to the preliminary conclusion that photochromism does not occur. Although the crystal structure indicates that the hydroxyl group on the non-color-changing compound molecule forms weak interactions with other atoms, thereby restricting the ESIPT process, photochromism does not occur. To directly observe the ESIPT process, we performed X-ray diffraction experiments on the crystals of the photochromic compound while continuously exposing them to ultraviolet light. Unfortunately, the resulting structure was identical to that of the unexposed sample, indicating that illumination only caused changes on the crystal surface without altering the internal structure or arrangement of the entire crystal. The proton transfer process cannot be observed from the crystal structure. To elucidate the color-changing mechanism, combining literature reports,[28–37,53–55] we propose that the photochromism of salicylaldehyde-aniline Schiff base involves a dual ESIPT + ISO process (Scheme 2). We then calculated the HOMO–LUMO energy levels and UV absorption spectra for the enol, *cis*-ketone, and *trans*-ketone forms of each compound (Table S7 and Fig. 4). Results indicate that the HOMO–LUMO energy gaps of these compounds show little variation. Following ESIPT, absorption peaks appear around 400 nm, and these peaks further intensify after the ISO process. This result aligns with solid-state UV measurements of photochromic compounds, indicating that all

compounds undergo color change following the ESIPT + ISO process. Consistent with literature reports, the mechanism for color change in these compounds involves the dual ESIPT + ISO process.

So, does the energy required for the ESIPT + ISO process remain the same? Therefore, we employed the Gaussian 16 software package to perform density functional theory (DFT) calculations at the B3LYP/6-31G(d) level of theory. This was done to elucidate the reaction mechanism of the double isomerization process in a series of tetraphenylethylene (TPE) derivatives. The optimized stable structures of enols, ketos, *trans*-ketos and the dual isomerization reaction energy barriers from enol to keto (TS1) and keto to *trans*-keto (TS2) are displayed in Fig S36–S38, Table S8 and S9, respectively. Notably, the isomerization from enol to keto are almost a barrierless process (TS1), **TPE-P** (0.21 kcal mol$^{-1}$), **TPE-o-FP** (0.64 kcal mol$^{-1}$), **TPE-p-MP** (0.64 kcal mol$^{-1}$), **TPE-p-FP** (0.79 kcal mol$^{-1}$), **TPE-p-tBuP** (0.15 kcal mol$^{-1}$), **TPE-o-BrP** (1.28 kcal mol$^{-1}$), **TPE-p-MOP** (0.27 kcal mol$^{-1}$), **TPE-p-NO$_2$P** (0.42 kcal mol$^{-1}$), indicating that the isomerization from enol to keto is nearly spontaneous.

After the formation of a series of ketone structures, the calculated keto-to-*trans*-keto rotational barriers (TS2) are 42.52 kcal mol$^{-1}$ for **TPE-P**, 42.27 kcal mol$^{-1}$ for **TPE-o-FP**, 42.39 kcal mol$^{-1}$ for **TPE-p-MP**, 42.92 kcal mol$^{-1}$ for **TPE-p-FP**, 41.94 kcal mol$^{-1}$ for **TPE-p-tBuP**, 42.08 kcal mol$^{-1}$ for **TPE-o-BrP**, 41.62 kcal mol$^{-1}$ for **TPE-p-MOP**, 45.49 kcal mol$^{-1}$ for **TPE-p-NO$_2$P**. Comparing with the energy barriers of enol-to-ketone, keto-to-*trans*-keto barriers are significantly higher (41.6–45.5 kcal mol$^{-1}$), peaking at 45.49 kcal mol$^{-1}$ for **TPE-p-NO$_2$P**, reflecting the steric-enhancing effect of strong electron-withdrawing groups. **TPE-o-FP** (42.27 kcal mol$^{-1}$) exhibits lower rotational barrier than its para-isomer (**TPE-p-FP**, 42.92 kcal mol$^{-1}$), revealing positional control over steric hindrance. Furthermore, the C1–C2–C3–N dihedral angle in the TS2 structure was twisted by approximately 84° relative to the keto, deviating from the anticipated 90° due to steric constraints, as shown in Fig. S38b. During the conversion from the keto to the *trans*-keto, the C2–C3 bond shortens while the C3–N bond elongates, suggesting a disruption of conjugation between the nitrogen atom and the benzene ring. The selected



**Scheme 2** Schematic illustration of the photochromic mechanism of salicylaldehyde–aniline Schiff bases.
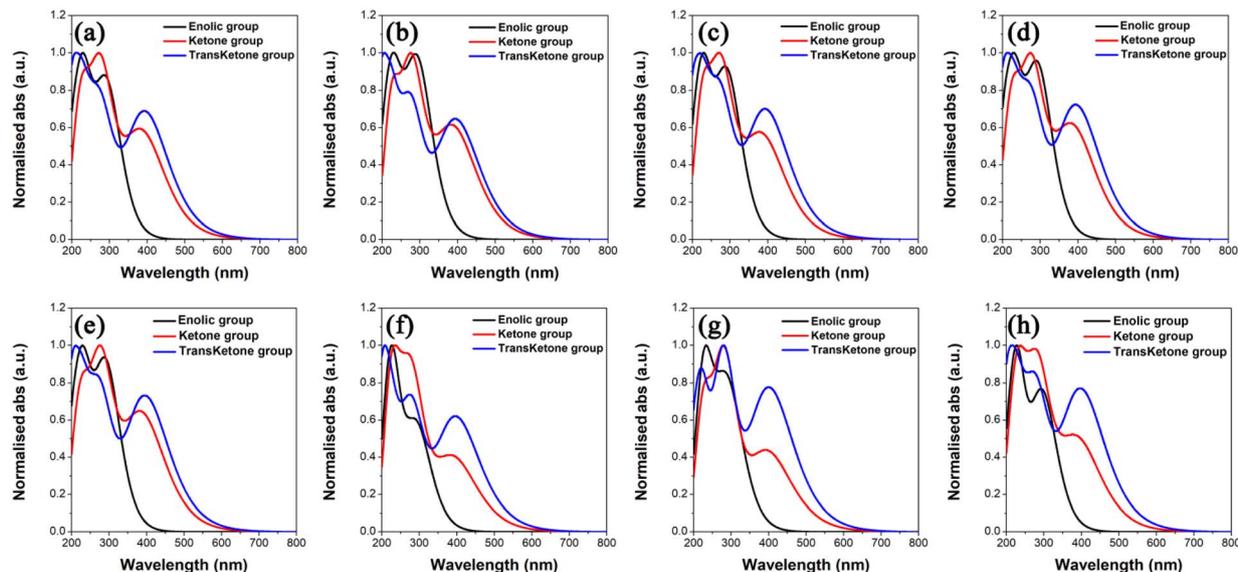
**Fig. 4** Theoretical UV-vis absorption spectra of the three configurations of compounds (a) TPE-P, (b) TPE-*p*-tBuP, (c) TPE-*o*-FP, (d) TPE-*p*-FP, (e) TPE-*p*-MP, (f) TPE-*p*-MOP, (g) TPE-*o*-BrP, and (h) TPE-*p*-NO$_2$P.

bond lengths and angles during keto-to-*trans*-keto conversion and the energy barriers of TS1 and TS2 are presented in Tables S8 and S9.

The above calculations indicate that the energy required for the ESIPT + ISO process in these eight compounds is essentially identical. This means that at the single-molecule level,

ultraviolet irradiation can induce the ESIPT + ISO process to achieve photochromism. Similar to reports,[28–37,53–55] this indicates that the aggregated state of molecules significantly influences the ESIPT process. Crystal structures serve as ideal models for studying aggregated states. Therefore, we conclude that compounds **TPE-*p*-tBuP**, **TPE-*o*-FP**, **TPE-*p*-FP**, and **TPE-*p*-**
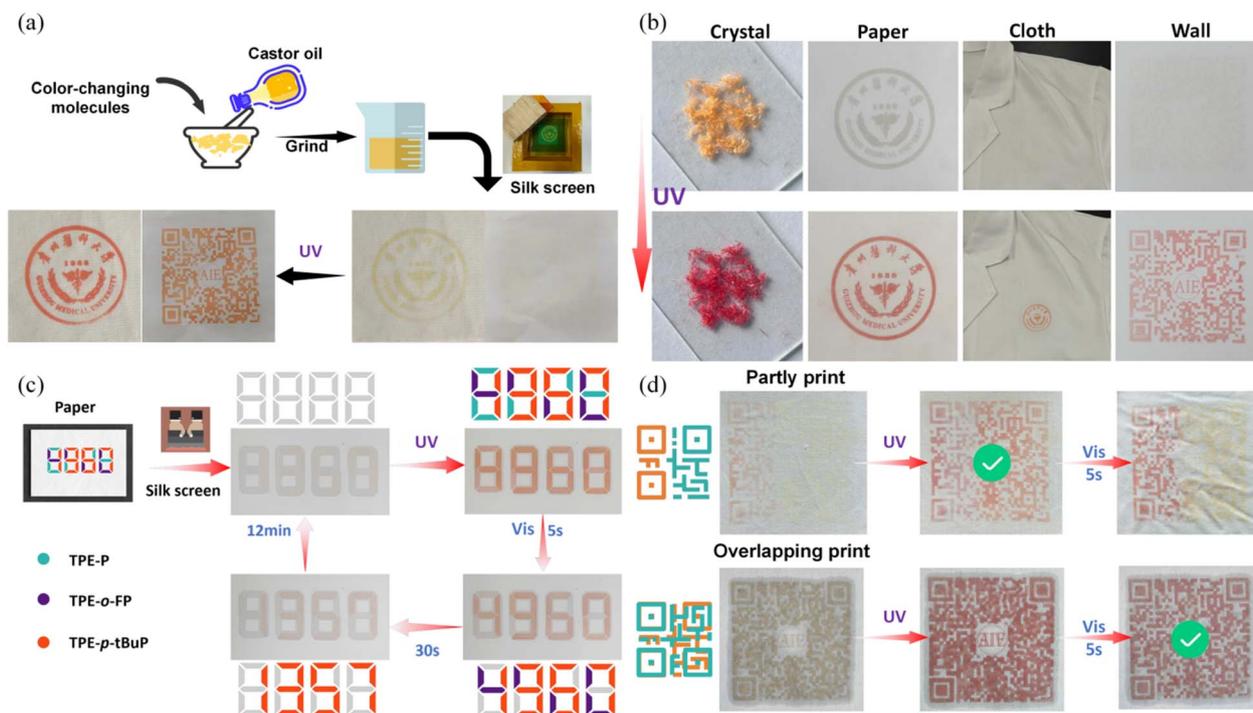


**Fig. 5** Information encryption and storage based on compound color change: (a) preparation of color-changing inks and their anti-counter-feiting performance; (b) anti-counterfeiting effects on various substrates; (c) time-encoded data storage and decryption; (d) QR code encryption and application demonstration.

**MP** undergo the ESIPT + ISO process upon UV irradiation to achieve color change. In contrast, compounds **TPE-*p*-MOP**, **TPE-*o*-BrP**, and **TPE-*p*-NO₂P** exhibit luminescence upon illumination rather than color change. This is because the hydroxyl group forms C–H⋯O weak interactions with other atoms in addition to the O1–H1⋯N1 hydrogen bond with the nitrogen atom of the C=N double bond, thereby restricting the ESIPT process.

### Application of color-changing encrypted anti-counterfeiting materials

Given the excellent photochromic properties of these compounds, their potential applications in information encryption and anti-counterfeiting were explored. Color-changing inks were prepared by grinding the photochromic compounds with mugwort and castor oil (Fig. 5a). The inks were used to print the Guizhou Medical University emblem and a personal QR code of Professor Qilong Zhang on paper. Upon UV irradiation, the printed patterns became clearly visible, and the QR code could still be scanned to access stored data. Similar encryption-decryption effects were achieved on textiles and inorganic substrates such as gypsum boards (Fig. 5b). These effects remained stable even after three years of storage (printed in 2022). Fabric samples printed with the photochromic inks retained full color-switching capability after five wash cycles using detergent (Tide Laundry Detergent), demonstrating the material's robustness and practical usability.

Next, color-changing inks derived from **TPE-P**, **TPE-*o*-FP**, and **TPE-*p*-tBuP**-which exhibit different fading durations—were combined to print the sequence "8888–4960–1357" in a designed pattern. As shown in Fig. 5c, immediately after UV exposure, all compounds were excited, displaying "8888". When **TPE-P** faded first, the visible pattern changed to "4960", and after **TPE-*o*-FP** faded, only **TPE-*p*-tBuP** remained, leaving "1357". By exploiting differences in fading times, temporal encryption of numerical data was achieved.

To test higher-dimensional encryption, QR codes were printed using **TPE-P** and **TPE-*p*-tBuP**—the compounds with the shortest and longest fading times—under two modes: half-printing and cross-overlay printing. The results are shown in Fig. 5d. In the half-printing mode, each ink covered half of the QR pattern without overlap, allowing it to be scanned immediately after UV exposure. When **TPE-P** faded, only the half containing **TPE-*p*-tBuP** remained, rendering the code unreadable. In contrast, in the cross-overlay mode, the overlapping inks initially interfered with one another, making the QR code unscannable under light exposure. After about 5 s, as **TPE-P** faded and interference disappeared, the section printed with **TPE-*p*-tBuP** became scannable, successfully revealing the encrypted information.

## Conclusions

In this study, an aldehyde–amine exchange strategy was employed based on the classical ESIPT + ISO color-switching mechanism of salicylaldehyde-aniline Schiff bases. Tetraphenylethyl salicylaldehyde was reacted with aniline derivatives bearing various substituents to synthesize eight tetraphenylethyl salicylaldehyde-aniline Schiff base compounds. Among them, five exhibited distinct photochromic behavior, while the remaining three showed strong solid-state fluorescence. Through a combination of spectroscopic analysis, theoretical calculations, and crystallographic characterization, the mechanisms responsible for color change and stability were elucidated. It was found that in the non-photochromic compounds, hydroxyl groups form additional weak interactions with nearby atoms, constraining the ESIPT process and thereby preventing color transition upon irradiation. This study constitutes the first systematic report on how substituent effects influence the ESIPT–ISO mechanism and demonstrates that weak intermolecular interactions and molecular packing can suppress ESIPT activity. It also represents the first investigation of substituent effects on the reverse ESIPT–ISO process. Finally, five photochromic materials were converted into color-shifting inks, enabling practical information encryption and anti-counterfeiting applications on paper, inorganic, and textile substrates through pad and screen printing. These printed materials maintained functionality for over three years of storage. Moreover, by exploiting differences in fading durations, multi-mode spatiotemporal data encryption and anti-counterfeiting were successfully achieved through controlled sequential printing of these color-changing inks.

## Author contributions

Q. Zhang. designed engineered the compounds and wrote the paper; X. Zhou., X. Shan., Y. Bao., F. He., H. Xu. and B. Zhu. performed the experiments; C. Zhu. provided guidance on the experiments and paper writing. All authors contributed to the general discussion.

## Conflicts of interest

There are no conflicts to declare.

## Data availability

CCDC 2486841–2486848 contain the supplementary crystallographic data for this paper[56a–h].

Supporting data have been included in the article's supplementary information(SI). Supplementary information: experimental section, NMR and HRMS spectra, X-ray crystallographic data, photophysical spectra, theoretical calculation data. See DOI: https://doi.org/10.1039/d6sc00735j.

## Acknowledgements

# Notes and references

1 Y. Lin, J. Ma, Y. Jia, C. Yu and J. Cheng, Deep learning-assisted methods for accelerating the intelligent screening of novel 2D materials: New perspectives focusing on data collection and description, *Chem. Rev.*, 2025, **529**, 216436.

2 Z. Chen, Y. Yuan, S. Liang, M. Wan, K. Li, W. Zhou, Y. Wang and Z. Wang, An automatic scientific data collection framework for materials science, *Comput. Mater. Sci.*, 2025, **252**, 113772.

3 L. Xu, L. Lu, N. Xu, J. Huang, G. Li, J. Wang, X. Hu, A. Guerrero, J. C. V. Reyes, X. Xu and Z. Han, Progressive Learning-Guided Discovery of Single-Atom Metal Oxide Catalysts for Acidic Oxygen Evolution Reaction, *Angew. Chem., Int. Ed.*, 2025, **64**, e202510965.

4 Y. Shen, X. Le, Y. Wu and T. Chen, Stimulus-responsive polymer materials toward multi-mode and multi-level information anti-counterfeiting: recent advances and future challenges, *Chem. Soc. Rev.*, 2024, **53**, 606–623.

5 Y. Sun, X. Le, S. Zhou and T. Chen, Recent Progress in Smart Polymeric Gel-Based Information Storage for Anti-Counterfeiting, *Adv. Mater.*, 2022, **34**, 202201262.

6 Y. Xie, X. Zhao, H. Wang, Y. Tian, C. Liu, J. Wu, J. Cui, Z. Zhou, J. Chen and X. Chen, Hydrogen Bond-Associated Photofluorochromism for Time-Resolved Information Encryption and Anti-counterfeiting, *Angew. Chem., Int. Ed.*, 2025, **64**, 202414846.

7 Y. Wu, X. Chen and W. Wu, Multiple Stimuli-Response Polychromatic Carbon Dots for Advanced Information Encryption and Safety, *Small*, 2023, **19**, 202206709.

8 X. Kang, K. Jiang, S. Ge, K. Wei, Y. Zhou, B. B. Xu, K. Wang and X. Zhang, Frontier in Advanced Luminescent Biomass Nanocomposites for Surface Anticounterfeiting, *ACS Nano*, 2025, **19**, 11547–11575.

9 Y. Dong, S. Feng, W. Huang and X. Ma, Algorithm in chemistry: molecular logic gate-based data protection, *Chem. Soc. Rev.*, 2025, **54**, 3681–3735.

10 J. Wang, M. Cui, J. Dong, H. Yao, X. Li and F. Wang, Recent progress of luminescent lanthanide-based metal-organic frameworks for anti-counterfeiting application, *Coord. Chem. Rev.*, 2025, **544**, 216976.

11 D.-X. Xia, C.-Y. Xu, D.-X. Pan, M.-F. Ye, R.-L. Lin and J.-X. Liu, A multi-stimuli-responsive supramolecular polymer from γ-Cyclodextrin and Viologen for dual-mode display and ammonia/amines sensing, *Chem. Eng. J.*, 2026, **530**, 173548.

12 L.-J. Wu, A. Deng, J.-X. Liu, R.-L. Lin, M.-F. Ye and G.-Z. Huang, Cucurbit[7]Uril-Based Supramolecular Polymers With Dual Photochromism and Fluorescence: From Host–Guest Design to Smart Applications, *Aggregate*, 2025, **6**, e70145.

13 X.-F. Wang, R.-L. Lin, W.-Q. Sun, J.-X. Liu, L.-X. Xu, C. Redshaw and X. Feng, Cucurbit[7]Uril-Based Self-Assembled Supramolecular Complex with Reversible Multistimuli-Responsive Chromic Behavior and Controllable Fluorescence, *Adv. Opt. Mater.*, 2024, **12**, 2400839.

14 S. Mollick and J.-C. Tan, Organic solid-state photochromism using porous scaffolds, *Nat. Rev. Mater.*, 2025, **10**, 519–535.

15 F. Hassan, Y. Tang, H. K. Bisoyi and Q. Li, Photochromic Carbon Nanomaterials: An Emerging Class of Light-Driven Hybrid Functional Materials, *Adv. Mater.*, 2024, **36**, 202401912.

16 Y. Tian, X. Xin, J. Hu, Z. Li, M. Liu and G. Fu, Highly Transparent Photochromic Coating with Excellent Dimming Capability Based on B–O–W Coordination Bonding Strategy, *Angew. Chem., Int. Ed.*, 2025, **64**, 202513064.

17 A. Julià-López, J. Hernando, D. Ruiz-Molina, P. González-Monje, J. Sedó and C. Roscini, Temperature-Controlled Switchable Photochromism in Solid Materials, *Angew. Chem., Int. Ed.*, 2016, **55**, 15044–15048.

18 J. Ding, Z. Huang, D. Zhang, Y. Qu, S. Zhang, C. Zhang, B. Fang, L. Li and W. Huang, Rational structural design of aromatic Azo photoactive small molecules for biomedical applications, *Chem. Soc. Rev.*, 2025, **54**, 10363.

19 X. Xu, I. Sahalianov, H. Sun, Z. Li, S. Wu, B. Jiang, H. Ågren, G. V. Baryshnikov, M. Zhang and L. Zhu, Rapidly Generated, Ultra-Stable, and Switchable Photoinduced Radicals: A Solid-State Photochromic Paradigm for Reusable Paper Light-Writing, *Angew. Chem., Int. Ed.*, 2025, **64**, e202422856.

20 Z. Guo, Y. Su, H. Zong, F. Zhou, M. Wang and G. Zhou, A Universal Strategy for Reversible Photochromism of Viologen Derivatives in Solutions, *Adv. Opt. Mater.*, 2024, **12**, 240791.

21 X. Hu, B. Fang, P. Li, J. Wang, J. Li, Y. Dai and M. Yin, Naphthalimide-Conjugated Spiropyran: Dual-State Emission and Photo-Responsive Dynamic Fluorescence Color for Information Encryption Application, *Adv. Funct. Mater.*, 2025, **35**, 2423793.

22 Y. Ma, G. Xiao, X. Fang, T. Chen and D. Yan, Leveraging Crystalline and Amorphous States of a Metal-Organic Complex for Transformation of the Photosalient Effect and Positive-Negative Photochromism, *Angew. Chem., Int. Ed.*, 2023, **62**, e202217054.

23 E. Jin, V. Bon, S. Das, A. D. D. Wonanke, M. Etter, M. A. Karlsen, A. De, N. Bönisch, T. Heine and S. Kaskel, Engineering Photoswitching Dynamics in 3D Photochromic Metal-Organic Frameworks through a Metal-Organic Polyhedron Design, *J. Am. Chem. Soc.*, 2025, **147**, 8568–8577.

24 Z. Han, M. He, J. Lehn and Q. Li, Intrinsically Adaptive Salicylaldimine: Mechanically and Thermally Induced Switching between Photochromism and Photoluminescence, *J. Am. Chem. Soc.*, 2025, **147**, 22053–22061.

25 X. Lu, K. Zhang, X. Niu, D. Ren, Z. Zhou, L. Dang, H. Fu, C. Tan, L. Ma and S. Zang, Encapsulation engineering of porous crystalline frameworks for delayed luminescence and circularly polarized luminescence, *Chem. Soc. Rev.*, 2024, **53**, 6694–6734.

26 W. Li, R. O. Al-Kaysi and C. J. Bardeen, Light-Controlled Reconfigurable Optical Structures Using Photomechanical Organic Crystals, *Angew. Chem., Int. Ed.*, 2025, e202516743.

27 L. Lan and H. Zhang, Red and Near-Infrared Emissive Organic Crystals: Molecular Design and Optoelectronic Applications, *Angew. Chem., Int. Ed.*, 2025, **64**, e202509140.

28 Y. Li, J. Fu, B. Yao, P. Zeng, Q. Peng, Y. Li, K. Li and S. Zang, Pressure-Triggered Photochromism in Chiral Salicylaldehyde Schiff Bases, *Chin. J. Chem.*, 2024, **42**, 2987–2992.

29 W. Zhong, J. Zhang, Y. Lin, S. Li, Y. Yang, W. Wang, C. Si, F. E. Kühn, Z. Zhao, X. Cai and B. Z. Tang, Multi-site isomerization of synergistically regulated stimuli-responsive AIE materials toward multi-level decryption, *Chem. Sci.*, 2024, **15**, 3920–3927.

30 H. Sun, C. Li, W. Yu, Y. Chen, Z. Sun, Z. Li, W. Huang, D. Wu and L. Zhu, Excited-state intramolecular proton transfer (ESIPT)-triggered photochromic materials, *Chin. Chem. Lett.*, 2025, 111971.

31 Z. Wang, C. Huang, J. Liu, Y. Zeng and R. Xiong, Salicylideneaniline is a Photoswitchable Ferroelectric Crystal, *Chem. Eur. J.*, 2021, **27**, 14831–14835.

32 A. Huang, J. Hu, M. Han, K. Wang, J. L. Xia, J. Song, X. Fu, K. Chang, X. Deng, S. Liu, Q. Li and Z. Li, Tunable Photocontrolled Motions of Anil-Poly(ethylene terephthalate) Systems through Excited-State Intramolecular Proton Transfer and Trans–Cis Isomerization, *Adv. Mater.*, 2021, **33**, 2005249.

33 Q. Qiao, C. Wang, H. Wang, Y. Ruan, W. Liu, J. Chen, Z. Wu, X. Liu and Z. Xu, Tail-Assisted Excited-State Intramolecular Proton Transfer (ta-ESIPT) Fluorophores: A Universal Ratiometric Platform for Hydration-Sensitive Biomolecular Imaging and Sensing, *J. Am. Chem. Soc.*, 2025, **147**, 15602–15613.

34 X.-M. Cai, Y. Lin, Z. Tang, X. Zhang, T. Mu, S. Huang, Z. Zhao and B. Z. Tang, Filling the gap between molecular and aggregate states: how does molecular packing affect photophysical properties?, *Chem. Eng. J.*, 2023, **451**, 138627.

35 S. Hasebe, Y. Hagiwara, J. Komiya, M. Ryu, H. Fujisawa, J. Morikawa, T. Katayama, D. Yamanaka, A. Furube, H. Sato, T. Asahi and H. Koshima, Photothermally Driven High-Speed Crystal Actuation and Its Simulation, *J. Am. Chem. Soc.*, 2021, **143**, 8866–8877.

36 X. Cai, Y. Lin, Y. Li, X. Chen, Z. Wang, X. Zhao, S. Huang, Z. Zhao and B. Z. Tang, BioAIEgens derived from rosin: how does molecular motion affect their photophysical processes in solid state?, *Nat. Commun.*, 2021, **12**, 1773.

37 G. Huang, Q. Xia, W. Huang, J. Tian, Z. He, B. S. Li and B. Z. Tang, Multiple Anti-Counterfeiting Guarantees from a Simple Tetraphenylethylene Derivative-High-Contrasted and Multi-State Mechanochromism and Photochromism, *Angew. Chem., Int. Ed.*, 2019, **58**, 17814–17819.

38 X. Cai, W. Zhong, Z. Deng, Y. Lin, Z. Tang, X. Zhang, J. Zhang, W. Wang, S. Huang, Z. Zhao and B. Z. Tang, A simple AIE-active salicylideneaniline towards bimodal encryption-decryption with unique ESIPT-inhibited amorphous state, *Chem. Eng. J.*, 2023, **466**, 143353.

39 F. Ma, S. Zhang, J. Jiang, Y. Liu, J. Sun, J. W. Y. Lam, Z. Zhao and B. Z. Tang, Aggregate Science: from Molecules, beyond Molecules, *Adv. Mater.*, 2024, **37**, 2414188.

40 H. Zheng, S. Li, M. Wu, Y. Kang, J. Li, Q. Liang, X. Zheng, D. Fang and L. Jin, Multi-stimuli responsive behaviors of two TPE-based tautomers in the solid state and in solution, *J. Mater. Chem. C*, 2020, **8**, 4246–4252.

41 Q. Yan and S. Wang, Fusion of aggregation-induced emission and photochromics for promising photoresponsive smart materials, *Mater. Chem. Front.*, 2020, **4**, 3153–3175.

42 L. Shen, C. Yu, H. Xie, N. Xu, H. Xu, Y. Huang, C. Redshaw, X. Feng and Q. Zhang, Naphthaldehyde-based Schiff base dyes: aggregation-induced emission and high-contrast reversible mechanochromic luminescence, *Mater. Chem. Front.*, 2022, **6**, 2491–2498.

43 X. Shan, X. Zhou, Q. Wang, L. Shen, H. Xu, C. Redshaw, X. Feng and Q. Zhang, New anti-counterfeiting materials based on hemicyanine dyes: $HSO_3^-/SO_3^{2-}$ encryption and UV light decryption, *J. Mater. Chem. C*, 2024, **12**, 19564–19569.

44 X. Shan, X. Zhou, Q. Wang, L. Shen, Z. Wang, H. Xu, X. Yang, C. Redshaw and Q. Zhang, A dual reversible-mode near-infrared AIE fluorescent probe: naked-eye identification and removal of $CN^-$ and $HSO_3^-/SO_3^{2-}$ anions from food and environmental samples, *Food Chem.*, 2025, **495**, 146487.

45 Z. Zhang, J. Yin, Q. Wang, X. Zhou, L. Shen, H. Xu, X. Yang, C. Redshaw and Q. Zhang, Effect of Extended π-Bridges and Molecular Charge on the Photodynamic Activity of Aggregation-Induced Emission Photosensitizers against Multidrug-Resistant Bacteria, *ACS Appl. Mater. Interfaces*, 2025, **17**, 33381–33394.

46 X. Liang, X. Shan, Z. Zhang, X. Zhou, L. Shen, H. Xu, Z. Wang, C. Redshaw and Q. Zhang, Spiropyran-based triphenylamine AIEgens: pH-responsive and light-activated mitochondria-targeted fluorescence imaging, *Bioorg. Chem.*, 2025, **156**, 108214.

47 Q. Zhang, X. Zhou, X. Zhang, L. Shen, H. Xu, Z. Wang, C. Huang, C. Redshaw and B. Zhu, Novel AIE [2+2] Schiff base macrocycles containing a 2,6-pyridylimide skeleton: Self-assembly and $Cu^{2+}$ sensing, *Microchem. J.*, 2024, **207**, 112009.

48 S. Peng, X. Zhou, Q. Wang, L. Shen, Z. Wang, H. Xu, X. Yang, C. Redshaw and Q. Zhang, Cationic AIEgens with large rigid π-planes: Specific bacterial imaging and treatment of drug-resistant bacterial infections, *Bioorg. Chem.*, 2025, **159**, 108412.

49 X. Zhou, L. Shen, X. Tan, X. Wang, X. Liang, X. Shan, H. Xu, Z. Wang, C. Redshaw and Q. Zhang, Novel triphenylamine-pyrene-based AIEgens: Specific detection and imaging of $H_2O_2$ in aqueous solution and cells, *J. Mol. Struct.*, 2024, **1318**, 139262.

50 X. Zhou, Q. Zhang, Q. Lin, X. Liang, C. Zhang, Z. Zhang, L. Shen, X. Yang, H. Xu, C. Redshaw and Q. Zhang, Novel spiropyran fluorescent probes based on ESIPT and ICT: pH Response & Cyanide Detection, *J. Mol. Struct.*, 2025, **1322**, 140429.

51 Q. Zhang, X. Zhou, Z. Zhang, L. Shen, Z. Wang, H. Xu, C. Redshaw and Q. Zhang, A Schiff base dual mode"Turn-

On" fluorescent probe for selective detection of HClO/ClO⁻ in buffer, *J. Mol. Struct.*, 2025, **1343**, 142876.

52 Q. Zhang, Y. Bao, X. Zhou, Q. Zhang, L. Shen, Z. Wang, X. Yang, C. Redshaw and H. Xu, A near-infrared fluorescence-enhanced AIE colourimetric/fluorescent probe: specific detection of CN⁻ in environmental, food and biological samples, *J. Mol. Struct.*, 2025, **1348**, 143548.

53 L. Wang, Y. Li, X. You, K. Xu, Q. Feng, J. Wang, Y. Liu, K. Li and H. Hou, An erasable photo-patterning material based on a specially designed 4-(1,2,2-triphenylvinyl)aniline salicylaldehyde hydrazone aggregation-induced emission (AIE) molecule, *J. Mater. Chem. C*, 2017, **5**, 65–72.

54 H. Sun, J. Li, F. Han, R. Zhang, Y. Zhao, B. Miao and Z. Ni, Reversible photochromic tetraphenylethene-based Schiff base: Design, synthesis, crystal structure and applications as visible light driven rewritable paper and UV sensor, *Dyes Pigm.*, 2019, **167**, 143–150.

55 M. Luo, Y. Liu, J. Zhao, L. Jiang, X. Chen, W. Li, Z. Yang, Q. Yan, S. Wang and Z. Chi, Magic tetraphenylethene Schiff base derivatives with AIE, liquid crystalline and photochromic properties, *Dyes Pigm.*, 2022, **202**, 110222.

56 (*a*) CCDC 2486841: Experimental Crystal Structure Determination, 2026, DOI: 10.5517/ccdc.csd.cc2pgrpm; (*b*) CCDC 2486842: Experimental Crystal Structure Determination, 2026, DOI: 10.5517/ccdc.csd.cc2pgrqn; (*c*) CCDC 2486843: Experimental Crystal Structure Determination, 2026, DOI: 10.5517/ccdc.csd.cc2pgrrp; (*d*) CCDC 2486844: Experimental Crystal Structure Determination, 2026, DOI: 10.5517/ccdc.csd.cc2pgrsq; (*e*) CCDC 2486845: Experimental Crystal Structure Determination, 2026, DOI: 10.5517/ccdc.csd.cc2pgrtr; (*f*) CCDC 2486846: Experimental Crystal Structure Determination, 2026, DOI: 10.5517/ccdc.csd.cc2pgrvs; (*g*) CCDC 2486847: Experimental Crystal Structure Determination, 2026, DOI: 10.5517/ccdc.csd.cc2pgrwt; (*h*) CCDC 2486848: Experimental Crystal Structure Determination, 2026, DOI: 10.5517/ccdc.csd.cc2pgrxv.